Doppler and Frequency-Offset Synchronization in Wideband OFDM

Arnt-Børre Salberg, *Member, IEEE*, and Ananthram Swami, *Senior Member, IEEE*

***Abstract*—When the orthogonal frequency-division multiplexing (OFDM) signal is appreciably wideband, as in underwater communications, a single Doppler-shift parameter is inadequate to model the Doppler effect, and a rate parameter is required as well. Such a model also accommodates nonsynchronized sampling of the received signal. We establish conditions for the identifiability of the Doppler parameters, and show how they affect the placement of null subcarriers (NSC). We derive the maximum-likelihood (ML) estimator and the corresponding conditional Cramér–Rao lower bound. We show that the vector formulation is amenable to estimation of signal parameters via rotational invariance techniques (ESPRIT) analysis, leading to a suboptimal but closed-form estimator. If the rate parameter is left uncompensated, we establish that the effective SNR is drastically reduced, which further leads to an increased bit error rate (BER). The ML estimator is demonstrated by numerical simulations that show that the performance of the estimator approaches the Cramér–Rao lower bound in the moderate-to-high SNR regions.**

***Index Terms*—Doppler effects, Estimation of signal parameters via rotational invariance techniques (ESPRIT), orthogonal frequency-division multiplexing (OFDM), synchronization, underwater acoustics, wideband.**

I. Introduction

ORTHOGONAL frequency-division multiplexing (OFDM) is a spectrally efficient channel-partitioning technique that transforms a frequency-selective channel into a set of frequency-flat channels, without requiring channel knowledge at the transmitter. The ease of implementation and the fine granularity that OFDM provides have led to its acceptance in many standards such as Digital Audio Broadcasting (DAB), Digital Video Broadcasting (DVB), European Telecommunications Standards Institute-High Performance Radio Local Area Network (ETSI-HyperLAN), MultiMedia Access Communications (MMAC), 802.11a and 802.16a. OFDM modulation consists of N subcarriers, equispaced at a separation of $\Delta f = B/N$, where B is the total system bandwidth, and Δf is less than the channel-coherence bandwidth. All subcarriers are mutually orthogonal over a time interval of length $T_s = 1/\Delta f$. Each subcarrier is modulated with symbols belonging to a quadratic-amplitude modulation (QAM) or phase-shift keying (PSK) constellation. The OFDM symbol is typically preceded by a cyclic prefix whose duration is longer than the delay spread of the propagation channel, so that interblock interference (IBI) can be easily removed, without affecting the orthogonality of the subcarriers.

However, the orthogonality of the OFDM subchannels is very sensitive to carrier frequency offset (CFO) and phase noise [11], and if orthogonality is lost, intercarrier interference (ICI) or crosstalk is induced, and the performance degrades. Therefore, it is of crucial importance to estimate and compensate such factors. Other drawbacks of OFDM include increased dynamic range (peak-to-average power ratio) [10] of the signal, since OFDM is a superposition of modulated symbol streams, and potential loss of multipath diversity [18].

Frequency offsets may arise due to motion-induced Doppler and/or mismatch in the frequencies of the local oscillators (LO) [10]. In a narrowband system, all subcarriers suffer from approximately the same Doppler shift, and most analyses make the narrowband assumption (see, e.g., [2] and references therein). The narrowband assumption may not always hold, for example, in the case of underwater acoustics communications (UAC) [7], [14], [16], [19]. In this case, Doppler translates each frequency component by a different amount, and we need to model the effects of Doppler as frequency (and time) scaling. In UAC, the random motion of sea surfaces and currents cause Doppler spread (in addition to the Doppler shift caused by the relative motions of the objects). However, we will assume that the Doppler spread is much smaller than the subcarrier bandwidth, so that Doppler spread effects can be ignored. An error in the receiver clock frequency, or a sampling-rate offset, will cause the spacing of the demodulating carriers to differ from those transmitted, and the duration of the integrate-and-dump process to differ from the reciprocal of the transmitted carrier spacing [12].

In this paper, we will study the effects of Doppler on wideband UAC OFDM systems, and sampling frequency offset on wideband OFDM systems in general. We will propose a model that incorporates the effect of Doppler and sampling frequency offset, and show how we can compensate for such effects. In order to compensate for the Doppler effects, estimates of the Doppler parameters are needed. By using null subcarriers (NSCs), we derive estimators of the Doppler parameters using maximum likelihood (ML) and the estimation of signal parameters via rotational invariance techniques (ESPRIT) algorithm. NSCs, often dictated by regulations, have also been used in narrowband OFDM for CFO estimation [2], [8], [23]. We will illustrate by means of numerical simulations that proper placement of the NSCs is crucial in order to obtain reliable estimates of the Doppler-rate parameter. Contrary to the CFO-only NSC-based schemes suggested, for example, in [8] and [23], we

Manuscript received October 28, 2003; revised November 5, 2004; accepted November 22, 2004. The editor coordinating the review of this paper and approving it for publication is R. Negi.

A.-B. Salberg is with the Institute of Marine Research, NO-9294 Tromsø, Norway (e-mail: arntbs@ieee.no).

A. Swami is with the U.S. Army Research Laboratory, Adelphi, MD 20784-1197 USA (e-mail: a.swami@ieee.org).

Digital Object Identifier 10.1109/TWC.2005.858337

derive estimators that need only one OFDM frame in order to estimate the Doppler parameters.

Notation: We will denote matrices and vectors in bold face, using capital letters for matrices and lower case letters for vectors. The transpose, conjugate transpose, conjugate, real part, imaginary part, pseudoinverse, and trace of a matrix $\mathbf{A}$ will be denoted by $\mathbf{A}^{\mathrm{T}}$, $\mathbf{A}^{\mathcal{H}}$, $\mathbf{A}^{*}$, $\overline{\mathbf{A}}$, $\widetilde{\mathbf{A}}$, $\mathbf{A}^{\dagger}$, and $\mathrm{Tr}\{\mathbf{A}\}$; $[\mathbf{A}]_{m,n}$ will denote its (m,n)th element, $\langle\mathbf{A}\rangle$, the subspace spanned by its columns, and $\mathbf{P}_A = \mathbf{A}\mathbf{A}^{\dagger}$, the projection matrix onto the subspace $\langle\mathbf{A}\rangle$.

II. Signal Model

The output of the IDFT at the transmitter can be written as

$$x[k] = \frac{1}{\sqrt{N}} \sum_{n\in\mathcal{N}_{\mathrm{a}}} S_n \mathrm{e}^{\frac{j2\pi nk}{N}}, \qquad 0 \le k < N-1$$

where S_n is the QAM (or PSK) subsymbol on the nth subcarrier, and $\mathcal{N}_{\mathrm{a}}$ the set of active subcarriers, $\mathcal{N}_{\mathrm{a}} \subset \{-N/2+1,\ldots,N/2\}$, with N denoting the total number of subcarriers. As in a standard OFDM system, we assume that a cyclic prefix of length L (longer than the length of the channel impulse response and transmit-and-receive pulse shapes) is inserted. This is readily accomplished by letting $k = -L,\ldots,N-1$. Typically, a cyclic postfix is also used, and an overlapped raised cosine taper is applied, followed by digital-to-analog conversion, and analog filtering/pulse shaping represented by $g_T(t)$ [10], [20], [21]. Choices of L and N are dictated by the delay spread, the desired frequency, and the channel coherence time T_{c} and coherence bandwidth B_{c}; an approximate upper bound is given by $L/N < 1/T_{\mathrm{c}}B_{\mathrm{c}}$.

Let T_{s} denote the OFDM symbol period. Then (at baseband), the nth subcarrier is at frequency $f_n = n\Delta f$, where $\Delta f = 1/T_{\mathrm{s}}$ is the subcarrier spacing. The continuous-time transmitted complex baseband OFDM pulse can then be described as

$$x_{\mathrm{c}}(t) = \frac{1}{\sqrt{N}} \sum_{n\in\mathcal{N}_{\mathrm{a}}} S_n \mathrm{e}^{j2\pi tn\Delta f} u_{T_{\mathrm{s}}'}(t+T_{\mathrm{pre}}) * g_T(t) \qquad (1)$$

where $*$ denote convolution, $u_T(t) = 1, 0 < t < T$, and zero otherwise. Furthermore, $T_{\mathrm{s}}' = T_{\mathrm{pre}} + T_{\mathrm{s}} + T_{\mathrm{post}}$ is the total length of the OFDM frame, T_{pre} is the length of the cyclic prefix, and T_{post} that of the cyclic postfix. The cyclic-prefix parameter is $L = \lceil NT_{\mathrm{pre}}/T_{\mathrm{s}}\rceil$. In order to restrict the transmitted signal to a bandwidth smaller than N/T_{s}, the set $\mathcal{N}_{\mathrm{a}}$ is chosen such that "guard-bands" are provided at the edges of the transmission spectrum. The out-of-band emission is further limited by using an appropriate analog-transmission filter $g_T(t)$.

Let v denote the (assumed constant) relative speed between the transmitter and receiver, and c, the speed of propagation. Let $\beta \triangleq v/c$ denote the relative Doppler shift, where v denotes the velocity along the radial component. For a single-passband frequency component f, the Doppler effect can be approximated as a frequency scaling $f' = f(1+\beta)$. This is often used as an approximation for narrowband signals in which the whole signal spectrum is translated by the same frequency as the carrier. In wideband signals, Doppler translates each frequency component by a different amount, and the Doppler effect is more accurately modeled as a complete time scaling of the signal waveform (e.g., [19]).

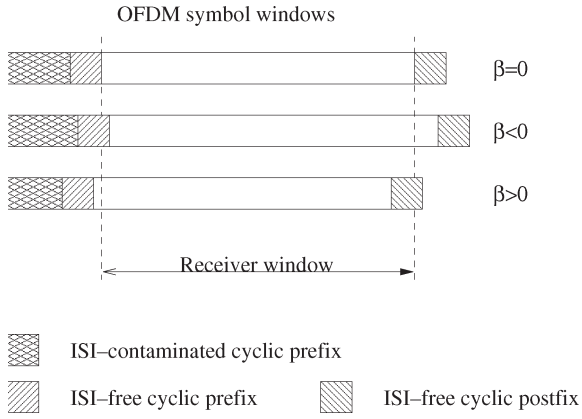

Fig. 1. OFDM-symbol window drift due to severe Doppler effects and/or sampling frequency offset.

Let f_{c} denote the carrier frequency, and f_{LO}, the frequency of the LO at the receiver. If we assume that the LO mismatch $f_{\mathrm{c}}(1+\beta) - f_{\mathrm{LO}}$ is a small fraction of the baud rate N/T_{s}, then the received OFDM pulse after the receiver filtering can be modeled as

$$y_{\mathrm{r}}(t) = \mathrm{e}^{j2\pi(f_{\mathrm{c}}(1+\beta)-f_{\mathrm{LO}})t} \left[h(t) * x_{\mathrm{r}}(t)\widetilde{u}_{T_{\mathrm{s}}'}(t)\right] + w(t)$$

where

$$x_{\mathrm{r}}(t) = \frac{1}{\sqrt{N}} \sum_{n\in\mathcal{N}_{\mathrm{a}}} S_n \mathrm{e}^{j2\pi n\Delta f(1+\beta)t}$$

$\widetilde{u}_{T_{\mathrm{s}}'}(t) = u_{T_{\mathrm{s}}'}(t(1+\beta))$, $h(t) = \widetilde{g}_T(t) * h_{\mathrm{c}}(t) * g_R(t)$, $\widetilde{g}_T(t) = g_T(t(1+\beta))$, and $g_R(t)$ and $h_{\mathrm{c}}(t)$ are the impulse responses of the receive filter and the continuous-time frequency-selective channel.

The apparent frequency (without CFO) of the nth subcarrier after downconversion to baseband at the receiver is

$$f_n' = (1+\beta)n\Delta f, \qquad n \in \mathcal{N}_{\mathrm{a}}.$$

Assume that (coarse) timing has been acquired, and that the cyclic prefix and postfix have been discarded. This operation is illustrated in Fig. 1, where we show the OFDM-symbol window drift due to severe Doppler effects (perfect timing synchronization is assumed for illustration purposes). In Fig. 1, we see that for $\beta < 0$, an ISI-free part of the cyclic prefix is necessary to avoid ISI from the previous OFDM symbol, whereas for $\beta > 0$, a cyclic postfix is necessary to avoid ISI from the next (!) OFDM symbol. Note that the cyclic prefix (the ISI-contained part in Fig. 1) is chosen longer than the memory of the channel. Then, in the interval $[0, T_{\mathrm{s}}]$, the received signal $y(t)$ can be modeled as

$$y(t) = \mathrm{e}^{j2\pi(f_{\mathrm{c}}(1+\beta)-f_{\mathrm{LO}})t} \left[h(t) * x_{\mathrm{r}}(t) + w(t)\right] u_{T_{\mathrm{s}}}(t), \qquad 0 \le t > T_{\mathrm{s}}. \qquad (2)$$

Since the continuous carriers $\mathrm{e}^{j2\pi f_n' t}$ are eigenfunctions of linear time-invariant (LTI) systems, i.e., $h(t) * \mathrm{e}^{j2\pi f_n' t} =$

$H(f_n')\mathrm{e}^{j2\pi f_n' t}$, where $H(f)=\mathcal{F}\{h(t)\}$ is the frequency response of the channel, the time-domain signal $y(t)$ can be expressed as

$$y(t)=\frac{1}{\sqrt{N}}\sum_{n\in\mathcal{N}_\mathrm{a}} H_n S_n \mathrm{e}^{j2\pi(n\Delta f+f_\mathrm{off})(1+\beta)t}+w(t),\qquad 0\le t<T_\mathrm{s}$$

where $f_\mathrm{off}=f_\mathrm{c}-f_\mathrm{LO}/(1+\beta)$, and $H_n=H((1+\beta)n\Delta f)=\int h(t)\exp(-j2\pi(1+\beta)n\Delta f t)\mathrm{d}t$.

The received signal is sampled at $t=kT=kT_\mathrm{s}/N=k/N\Delta f$, leading to the discrete-time equivalent model

$$y[k]=\frac{\mathrm{e}^{\frac{j2\pi k\delta}{N}}}{\sqrt{N}}\sum_{n\in\mathcal{N}_\mathrm{a}} H_n S_n \mathrm{e}^{\frac{j2\pi kn(1+\beta)}{N}}+w[k] \tag{3}$$

where

$$\delta\triangleq\frac{f_\mathrm{off}(1+\beta)}{\Delta f}=\frac{(1+\beta)f_\mathrm{c}-f_\mathrm{LO}}{\Delta f} \tag{4}$$

denotes the normalized shift of the carrier, and $w[k]$ is modeled as zero-mean complex additive white Gaussian noise. The model in (3) also accommodates a sampling frequency offset. If the received signal is sampled at $t=kT(1+\epsilon)$, where ϵ is the relative error, then (3) becomes

$$y[k]=\frac{\mathrm{e}^{\frac{j2\pi k\delta(1+\epsilon)}{N}}}{\sqrt{N}}\sum_{n\in\mathcal{N}_\mathrm{a}} H_n S_n \mathrm{e}^{\frac{j2\pi kn(1+\beta)(1+\epsilon)}{N}}+w[k]$$

which is in the same form as (3).

In UAC, acoustic reverberations can lead to extremely long channel impulse responses, and therefore, channel shortening may be needed in order to reduce the channel delay spread, and ensure that the length of the cyclic prefix is greater than the channel delay spread [1], [9]. This can be ensured, for example, by using a time-domain equalizer in the receiver front end.

Clearly, a $\beta\neq 0$ results in nonsynchronized sampling of the received OFDM signal. This nonsynchronized sampling results in a drift in the symbol timing and can further worsen the symbol-synchronization problem. The symbol-timing errors will be linearly increased or decreased, which requires that at regular intervals, samples must be robbed (if $\beta>0$) or stuffed (if $\beta<0$) [12]. If we consider OFDM with $N=256$ subcarriers, the OFDM symbol drift will be ± 1 sample per OFDM symbol if $\beta=0.0039$. Such a β is obtained in the UAC case with $c=1500$ m/s and $v=21$ km/h. To exemplify the importance of this, let us consider two cases.

1) In UAC, the speed of sound in water is approximately $c=1500$ m/s; for a reasonable mobile velocity of 10 km/h, we obtain $\beta\approx 2\times 10^{-3}$. In the case of radio-frequency (RF) communications, with $c=3\times 10^8$ m/s, and $v=100$ km/h, $\beta\approx 10^{-7}$. Clearly, we expect the Doppler effects to be larger for UAC than for RF ultrawideband (RF-UWB) communications.
2) The Federal Communications Commission (FCC) sanctioned RF-UWB spectrum ranges from 3.1 to 10.6 GHz [13]; with $v=100$ km/h, the Doppler shifts are 310 and 1060 Hz at the two ends of the spectrum. Is this difference significant? If the subchannel spacing is large, say 200 kHz, then the range of Doppler shifts is not important. If the channel spacing becomes smaller, say 20 kHz, then the range becomes important. Considering the number of subcarriers this implies, it is unlikely that the multiband OFDM proposed in 802.15.3a will follow the conventional OFDM format over the entire bandwidth.

III. Analysis of the Discrete-Time Model

The discrete-time model of the received signal in (3) can be written in vector-matrix form as

$$\mathbf{y}=\mathbf{D}(\delta)\mathbf{F}_\beta^H\mathbf{T}_\mathrm{a}\boldsymbol{\alpha}+\mathbf{w} \tag{5}$$

where $\mathbf{y}=[y[0]\ \ldots\ y[N-1]]^\mathrm{T}$, $\mathbf{D}(\delta)=\mathrm{diag}(1,\mathrm{e}^{j2\pi\delta/N},\ldots,\mathrm{e}^{j2\pi\delta(N-1)/N})$

$$\begin{aligned}\boldsymbol{\alpha}&=\left[\alpha_{n_1}\ \cdots\ \alpha_{n_{N_\mathrm{a}}}\right]^\mathrm{T}\\&=\left[S_{n_1}H_{n_1}\ \cdots\ S_{n_{N_\mathrm{a}}}H_{n_{N_\mathrm{a}}}\right]^\mathrm{T}\end{aligned} \tag{6}$$

$$\left[\mathbf{F}_\beta^H\right]_{k,n}=\frac{1}{\sqrt{N}}\exp\left(\frac{j2\pi kn(1+\beta)}{N}\right) \tag{7}$$

and $k=0,\ldots,N-1$, $n=-N/2+1,\ldots,N/2$. The matrix $\mathbf{T}_\mathrm{a}$ is an $N\times N_\mathrm{a}$ selection matrix, with $[\mathbf{T}_\mathrm{a}]_{k,\ell}=1$ if the ℓth symbol is on subcarrier k. Clearly, if $\beta=0$, then $\mathbf{F}_\beta^{\mathcal{H}}=\mathbf{F}_0^{\mathcal{H}}=\mathbf{F}^{\mathcal{H}}$, i.e., the IDFT matrix, and we have a standard CFO problem. Defining

$$\mu_N(\theta)\triangleq\frac{1}{N}\sum_{n=0}^{N-1}\mathrm{e}^{\frac{j2\pi n\theta}{N}}=\mathrm{e}^{\frac{j\pi\theta(N-1)}{N}}\frac{1}{N}\frac{\sin(\pi\theta)}{\sin\left(\frac{\pi\theta}{N}\right)}$$

we see that the (m,n)th entry of $\mathbf{F}_\beta\mathbf{F}_\beta^{\mathcal{H}}$ is $\mu_N((1+\beta)(n-m))$, so that the columns of $\mathbf{F}_\beta^{\mathcal{H}}$ are not orthogonal in general. Thus, even if we compensate for $\mathbf{D}(\delta)$, applying the DFT operator ($\mathbf{F}_\beta$ or $\mathbf{F}$) to the received vector $\mathbf{y}$ will introduce ICI. To avoid this, one must compute and apply $\mathbf{F}_\beta^{-\mathcal{H}}$; since $\mathbf{F}_\beta$ is Vandermonde, computation and application of the inverse can be done in $O(N^2)$ flops.

If δ and β in (5) are known, we will show in Section V that the ML estimate of the faded symbol $\boldsymbol{\alpha}$ (treated as nonrandom) is given by $(\mathbf{F}_\beta^{\mathcal{H}}\mathbf{T}_\mathrm{a})^\dagger\mathbf{D}^{\mathcal{H}}(\delta)\mathbf{y}$. If $\mathbf{F}_\beta^{\mathcal{H}}\mathbf{T}_\mathrm{a}$ does not have full column rank, then the faded-symbol vector $\boldsymbol{\alpha}$ cannot be recovered. Since $\mathbf{T}_\mathrm{a}$ has full column rank, we identify the conditions under which $\mathbf{F}_\beta^{\mathcal{H}}$ becomes singular.

In UAC, $c\approx 1500$ m/s; for a relative speed of $v=10$ m/s, $\beta=v/c\ll 1$, which is typical. Hence, we will confine the analysis to $|\beta|<1$.

Proposition 1: For $|\beta|<1$, matrix $\mathbf{F}_\beta^{\mathcal{H}}$ is singular if and only if (IFF)

$$\beta=\frac{p}{N-p},\qquad 1\le p<\frac{N}{2} \tag{8}$$

in which case $\mathrm{rank}\{\mathbf{F}_\beta^{\mathcal{H}}\}=N-p$, $p\in\mathbb{N}$.

Proof: Matrix $\mathbf{F}_\beta^{\mathcal{H}}$ is Vandermonde with generators $\exp(j2\pi k(1+\beta)/N)$, $k=-N/2+1,\ldots,N/2$. This matrix has full rank IFF the generators are distinct, i.e., $\exp(j2\pi(k-\ell)(1+\beta)/N)\neq 1$, if $k\neq \ell \bmod N$. Equivalently, the matrix loses rank IFF there exist integers n and m, with $0<m<N$, such that $m(1+\beta)/N=n$, i.e., $\beta=(nN/m)-1$. If $-1<\beta<0$, then the matrix loses rank IFF $-1<nN/m-1<0$, i.e., $0<nN/m<1$. But with $0<m<N$, this is impossible for any integer n. If $0<\beta<1$, the matrix loses rank IFF $0<(nN/m)-1<1$ i.e., $1<nN/m<2$. Since $m<N$, it follows that $n=1$. Furthermore, $1<N/m<2$, implies that $N/2<m<N$. Now, $\beta=N/m-1=(N-m)/m=\ell/(N-\ell)$, with $0<\ell<N/2$. But the generators are $\exp(j2\pi k(1+\beta)/N)=\exp(j2\pi k/(N-\ell))$, $k=0,\ldots,N-1$, so that the matrix has rank $N-\ell(>N/2)$. Hence, with $|\beta|<1$, the matrix loses rank only at the $N/2-1$ distinct values, $\beta=\ell/(N-\ell)$, $0<\ell<N/2$. Thus, the matrix has rank $N-\ell$. ■

Remarks:

1) When $\beta=\ell/(N-\ell)$, the first ℓ columns of $\mathbf{F}_\beta$ are identical to the last ℓ columns. Hence, either the leading or trailing set of ℓ carriers must be left unmodulated. The minimum number of guard-band subcarriers required is $p_{\min}=\lceil N\beta/(1+\beta)\rceil$. For the RF-UWB case, this works to 1, even with $\Delta f=25$ kHz. For the underwater acoustics example considered earlier, we get $p_{\min}=2$. So, the good news is that, in practice, symbol identifiability is always ensured, without imposing extra requirements on the transmission scheme or on the receiver.
2) An interesting property of $\mathbf{F}_\beta^{\mathcal{H}}$ is that if $\beta=p/(N-p)$, $1\leq p<N/2$, then any $(N-p)\times(N-p)$ submatrix $\mathbf{G}$ of $\mathbf{F}_\beta^{\mathcal{H}}$ is orthogonal, i.e., $\mathbf{G}^{\mathcal{H}}\mathbf{G}=(N-p)/N\mathbf{I}_{N-p}$.
3) Identifiability of $\boldsymbol{\alpha}$ is possibly lost only for $\beta>0$, i.e., when the transmitter and receiver are moving toward each other. Note also that the rank condition is only a sufficient condition for symbol identifiability, since $\mathbf{F}_\beta^{\mathcal{H}}\mathbf{T}_{\mathrm{a}}$ may have full column rank, even if $\mathbf{F}_\beta^{\mathcal{H}}$ is singular.
4) For general β, the matrix loses rank only if $\beta=-1\pm mN/k$, $0<k\leq N-1$, and m is an integer.

A. Subcarrier Selection

Proposition 1 indicates that symbol recovery may not be possible under some conditions, even when δ and β are known exactly. If β is known before sampling, one can sample at $t=kT_{\mathrm{c}}/(1+\beta)$, in which case the problem reduces to a solved problem corresponding to $\beta=0$ [2]. In practice, one must estimate (and possibly track) β and δ on a (OFDM) symbol-by-symbol basis. To ensure symbol recovery, independent of β, we must design the subcarrier selection matrix $\mathbf{T}_{\mathrm{a}}$ carefully.

Remark 1 above indicates the minimum number of guard-band subcarriers required to ensure symbol identifiability. Proposition 1 indicates when the matrix loses rank. The matrix becomes ill-conditioned when β is close to any of the critical values $p/(N-p)$, but can be conditioned by adding a few NSCs at the band edges. In practice, we expect $|\beta|<0.01$. In this range, the matrix is very well behaved, with condition numbers less than 10.

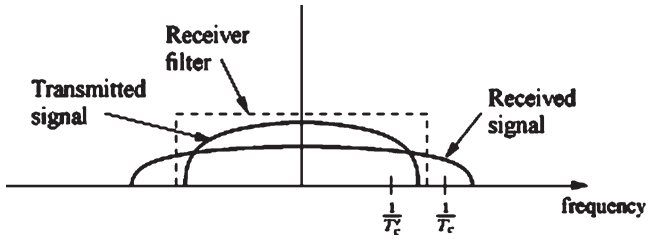

Fig. 2. Illustration of the effect of $\beta>0$.

B. Physical Interpretations

For $\beta\in(0,1)$, we have that $|f_n'|>|f_n|$, $\forall n$, and the signal spectrum is expanded by a factor $(1+\beta)$. Since the OFDM signal is sampled at a frequency $1/T_{\mathrm{c}}=2f_{N/2}$, aliasing will result. If β is of the form $\beta=p/(N-p)$, $1\leq p<N/2$, the aliased frequency components will perfectly align with some nonaliased frequency components, leading to a loss of rank in $\mathbf{F}_\beta^{\mathcal{H}}$, and thus, symbol identifiability. For other values of β, we should expect some degradation since the modulated subcarriers have nonzero bandwidth.

Clearly, for $\beta\in(-1,0)$ we have that $|f_n'|<|f_n|$, and the signal spectrum is compressed along the frequency axis. In this case, the sampling frequency $1/T_{\mathrm{c}}>2f_{N/2}'$, and no aliasing occurs.

Note that if $\beta>0$ is due to a Doppler shift of the received signal, then the frequency components higher than the sampling frequency $1/T_{\mathrm{c}}$ will be suppressed by the antialiasing filter at the receiver (see Fig. 2). If $\beta>0$ is due to a sampling frequency offset, such that the offset sampling frequency $1/T_{\mathrm{c}}'$ is lower than the band-edge frequency of the antialiasing filter (see Fig. 2), then $\boldsymbol{\alpha}$ could be nonidentifiable due to aliasing. In addition, frequency components in the additive noise will be aliased, although this will only cause the noise to become correlated.

The antialiasing filter will also suppress frequency components larger than $1/T_{\mathrm{c}}$ in the received signal if the shift parameter δ is larger than the guard bands. Hence, guard bands should be selected sufficiently large to cope with frequency spectrum shifts due to Doppler and LO mismatch.

C. Subcarrier-Interference Analysis

Assume that the received discrete-time signal $y[k]$ is given by (3). Then, the outputs of the DFT demodulator (indexed by $\ell\in\mathcal{N}_{\mathrm{a}}$) for one OFDM symbol are

$$\begin{aligned} z[\ell] &= \frac{1}{\sqrt{N}}\sum_{k=0}^{N-1} y[k]\mathrm{e}^{\frac{-j2\pi k\ell}{N}}+\overline{w}[\ell] \\ &= H_\ell S_\ell \mu_N(\delta+\ell\beta) \\ &\quad + \sum_{\substack{n\in\mathcal{N}_{\mathrm{a}}\\ n\neq\ell}} H_n S_n \mu_N\left(\delta+n(1+\beta)-\ell\right)+\overline{w}[\ell] \end{aligned} \quad (9)$$

which can be written in vector–matrix form as $\mathbf{z}=\mathbf{F}_0\mathbf{D}(\delta)\mathbf{F}_\beta^H\mathbf{T}_{\mathrm{a}}\boldsymbol{\alpha}+\tilde{\mathbf{w}}$.

In general, the matrix $\mathbf{F}_0\mathbf{D}(\delta)\mathbf{F}_\beta^H$ is not diagonal. Thus, the DFT output consists of a desired term, a linear subcarrier

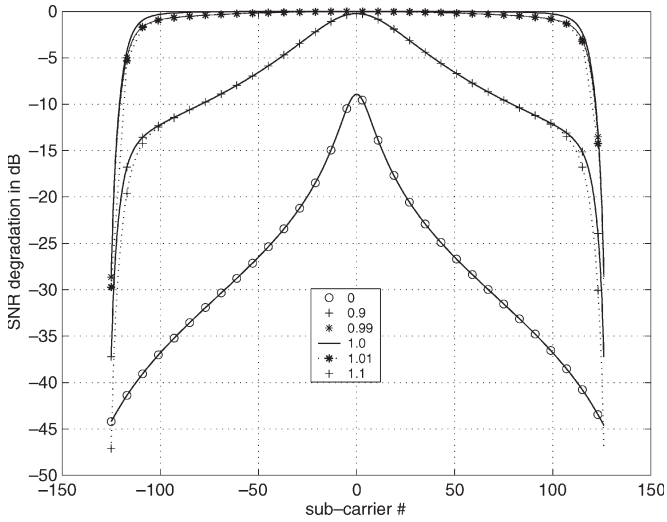

Fig. 3. Effective SNR versus subcarrier index for $N = 256$, four NSCs, $\beta = 1/150$, $\delta = 0$, and $\sigma_w^2 = -30$ dB, when the received data are processed with $(\mathbf{F}_{\hat{\beta}}^{\mathcal{H}})^{\dagger}$, for different values of $\hat{\beta}/\beta$.

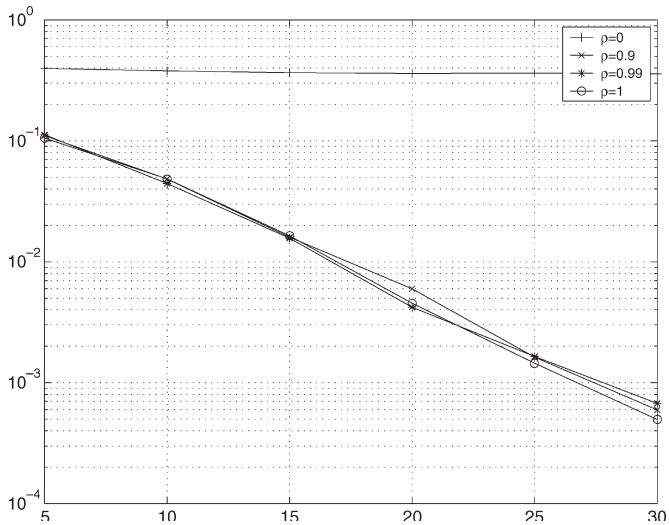

Fig. 4. BER versus as a function of SNR evaluated for $\widehat{\beta} = \rho\beta$. The $(+)$-, $(\times)$-, (o)-, and $(*)$-curve correspond to $\rho = 0$, 0.90, 1, and 0.99, respectively.

interference term, and an additive noise term $\overline{w}[\ell]$. This scenario corresponds to the case where the receiver ignores the Doppler. We can follow the approach of [22] to characterize the interference. The signal-to-subcarrier-interference ratio for subcarrier number ℓ is

$$\gamma(\ell) = \frac{\sigma_{\mathrm{s}}^2(\ell)\sigma_H^2(\ell)\,|\mu_N(\delta+\ell\beta)|^2}{\sum\limits_{\substack{n\in\mathcal{N}_{\mathrm{a}}\\ n\neq\ell}} \sigma_{\mathrm{s}}^2(\ell)\sigma_H^2(n)\,|\mu_N(\delta+n(1+\beta)-\ell)|^2} \tag{10}$$

where $\sigma_h^2(n) = \mathrm{Var}\{H_n\}$ and $\sigma_{\mathrm{s}}^2(n) = \mathrm{Var}\{S_n\}$. In deriving this, we have assumed that the channel coefficients H_n are independent of the symbols, which are i.i.d. (no coding across subcarriers). The derivation holds for a coded system, if the channel fades are uncorrelated, but can be easily extended to the correlated case. The effective SNR for each subcarrier is

$$\mathrm{SNR}_e(\ell) = \frac{\sigma_{\mathrm{s}}^2(\ell)\sigma_H^2(\ell)\,|\mu_N(\delta+\ell\beta)|^2}{\sum\limits_{\substack{n\in\mathcal{N}_{\mathrm{a}}\\ n\neq\ell}} \sigma_{\mathrm{s}}^2(\ell)\sigma_H^2(n)\,|\mu_N\,(\delta+n(1+\beta)-\ell)|^2+\sigma_w^2} \tag{11}$$

where $\sigma_w^2 = \mathrm{Var}\{W_\ell\} = \mathrm{E}\{|W_\ell|^2\}$.

Fig. 3 depicts the SNR degradation versus the subcarrier index n for $\beta = 1/150$, $N = 256$, $\delta = 0$, $\sigma_H^2(n) = 1$, $\sigma_{\mathrm{s}}^2(\ell) = 1$, $\sigma_w^2 = 10^{-3}$, for various estimated values of β. The (o)-curve shows the SNR degradation when $\mathbf{F}$ is applied, i.e., $\beta = 0$ is assumed. Notice the substantial degradation, particularly for large $|n|$, and that subcarriers with $|n| > 50$ have an SNR loss larger than 25 dB. The different curves correspond to processing the data using an estimated $\hat{\beta} = \rho\beta$, i.e., $(\mathbf{F}_{\hat{\beta}}^{\mathcal{H}})^{\dagger}$ is used. The solid line corresponds to $\rho = 1$, i.e., perfect estimation; in this case, there is no ICI, and the curve is flat at the SNR degradation of 0 dB, except at the band edges ($|n| > 100$). This is because we are processing the received data with $(\mathbf{F}_{\beta}^{\mathcal{H}})^{\dagger}$, which amplifies the additive noise substantially at the highest frequencies. The solid $+$ and $*$ curves correspond to $\rho = 0.9$ and 0.99, and the dashed $+$ and $*$ correspond to $\rho = 1.1$ and $\rho = 1.01$. An accuracy of 1% in estimating β appears to give adequate SNR degradation for most of the active subcarriers in this scenario. The degradation due to overestimation of β rather than underestimation (e.g., 1.1 versus 0.9) is minor. Similar curves were obtained for other values of σ_w^2, but Doppler-related effects were observed to be more significant at higher SNR.

To demonstrate the impact that a $\beta = 1/150$ has on the performance, we show in Fig. 4 the bit error rate (BER) as a function of SNR evaluated for various estimated values of β. The data symbols are drawn from a QPSK constellation, and the channel coefficients $\{h_\ell\}, \ell = 0, \ldots, L_h$, with $L_h = 16$, are generated using an uncorrelated Rayleigh-scattering model with a flat power-delay profile, i.e., $\mathrm{E}\{h_k^* h_\ell\} = \sigma_h^2\delta_{k,\ell}$. A single-tap minimum-mean-square-error (MMSE) equalizer, based on known channel coefficients and a postulated β parameter, was used, $\mathbf{G}(\mathbf{F}_{\hat{\beta}}^{\mathcal{H}}\mathbf{D}(\mathbf{H}))$ where $\mathbf{G}(\mathbf{A}) := (\mathbf{A}^{\mathcal{H}}\mathbf{A} + \sigma_w^2\mathbf{I})^{-1}\mathbf{A}^{\mathcal{H}}$. The $(+)$-curve shows the BER when $\mathbf{F}$ is applied. The $(\times)$- and $(*)$-curves correspond to processing the data assuming $\hat{\beta} = \rho\beta$, i.e., instead of processing the data with $\mathbf{F}$, we process it with $(\mathbf{F}_{\hat{\beta}}^{\mathcal{H}})^{\dagger}$. The $(\times)$-curve corresponds to $\rho = 0.90$, the $(*)$-curve to $\rho = 0.99$, and the (o)-curve to $\rho = 1$. We see that processing the data with $\mathbf{F}$ leads to a substantial degradation in performance. Since $\mathbf{F}_\beta$ is not orthogonal, the MMSE receiver involves an explicit matrix inversion (once per channel or β parameter update), and obviates some of the low-complexity equalizer advantages of narrowband OFDM. One might be tempted to use the equalizer $\mathbf{G}(\mathbf{D}(\mathbf{H}))\mathbf{F}_{\hat{\beta}}$. Doing this leads to about a 3-dB degradation in BER with $\rho = 0.9$ at high SNR. Thus, we observe that an accuracy of 10% in estimating β appears to cause only a small degradation in the BER in this scenario, and an accuracy of 1% in estimating β barely degrades the BER.

The preceding analysis and figures indicate that we need good estimates of β. Can we obtain good estimates? In order to answer this, we look at performance bounds, namely the Cramér–Rao bound (CRB). A second issue is to develop low-complexity estimators.

IV. Cramer–Rao Bounds (CRBs)

The unknown parameters are δ, β, and $\alpha_n, n \in \mathcal{N}_\mathrm{a}$, where $\alpha_n = H_n S_n$. The α_n's are nuisance parameters and are modeled as nonrandom. The corresponding CRB will be referred to as the conditional CRB (CCRB), since the α_n's are treated as deterministic constants. The CCRB is the inverse of the conditional Fisher information matrix. We will find it convenient to define

$$\mathbf{\Phi}_\mathrm{a}(\beta) \triangleq \mathbf{F}_\beta^{\mathcal{H}} \mathbf{T}_\mathrm{a}. \tag{12}$$

We will assume that $\mathbf{F}_\beta^{\mathcal{H}}$ has full rank, i.e., $\beta \neq \ell/(N-\ell)$; hence, $\mathbf{\Phi}_\mathrm{a}(\beta)$ also has full rank.

Proposition 2: For the model in (5), the CCRBs are given by

$$\mathrm{CCRB}(\beta) = \frac{C_\delta}{C_\delta C_\beta - C_{\delta,\beta}^2}, \quad \mathrm{CCRB}(\delta) = \frac{C_\beta}{C_\delta C_\beta - C_{\delta,\beta}^2} \tag{13}$$

where the FIM elements are

$$\begin{aligned}
C_\beta &= \frac{N^2}{2\pi^2 \sigma_w^2} \sum_{k=0}^{K-1} \boldsymbol{\alpha}_k^{\mathcal{H}} \mathbf{Q}_\mathrm{a}^{\mathcal{H}} \mathbf{\Phi}_\mathrm{a}^{\mathcal{H}}(\beta) \mathbf{Q}^{\mathcal{H}} \\
&\quad \times \left[\mathbf{I} - \mathbf{P}_{\Phi_\mathrm{a}}(\beta)\right] \mathbf{Q} \mathbf{\Phi}_\mathrm{a}(\beta) \mathbf{Q}_\mathrm{a} \boldsymbol{\alpha}_k, \\
C_\delta &= \frac{2}{\sigma_w^2} \sum_{k=0}^{K-1} \boldsymbol{\alpha}_k^{\mathcal{H}} \mathbf{\Phi}_\mathrm{a}^{\mathcal{H}}(\beta) \mathbf{Q}^{\mathcal{H}} \\
&\quad \times \left[\mathbf{I} - \mathbf{P}_{\Phi_\mathrm{a}}(\beta)\right] \mathbf{Q} \mathbf{\Phi}_\mathrm{a}(\beta) \boldsymbol{\alpha}_k, \\
C_{\delta,\beta} &= \frac{N}{\pi \sigma_w^2} \sum_{k=0}^{K-1} \Re\big\{(-1) \boldsymbol{\alpha}_k^{\mathcal{H}} \mathbf{\Phi}_\mathrm{a}^{\mathcal{H}}(\beta) \mathbf{Q}^{\mathcal{H}} \left[\mathbf{I} - \mathbf{P}_{\Phi_\mathrm{a}}(\beta)\right] \\
&\qquad \times \mathbf{Q} \mathbf{\Phi}_\mathrm{a}(\beta) \mathbf{Q}_\mathrm{a} \boldsymbol{\alpha}_k \big\}, \\
\mathbf{Q} &= \frac{j2\pi}{N} \mathrm{diag}\left[0, 1, \ldots (N-1)\right], \\
\mathbf{Q}_\mathrm{a} &= \frac{j2\pi}{N} \left[-\frac{N_\mathrm{a}}{2} + 1, \ldots, \frac{N_\mathrm{a}}{2}\right], \\
\mathbf{P}_{\Phi_\mathrm{a}}(\beta) &\triangleq \mathbf{\Phi}_\mathrm{a}(\beta) \mathbf{\Phi}_\mathrm{a}(\beta)^\dagger.
\end{aligned}$$

See Appendix for an outline of the proof. ■

Observations:

1) The CCRBs of β and δ do not depend on the shift parameter δ, only on the rate parameter β.
2) Since we assume that $\mathbf{\Phi}_\mathrm{a}(\beta)$ has full column rank, the matrix $\mathbf{P}_{\Phi_\mathrm{a}}(\beta)$ is the projection matrix onto the subspace spanned by the columns of $\mathbf{\Phi}_\mathrm{a}(\beta)$. However, if $\mathbf{\Phi}_\mathrm{a}(\beta)$ does not have full column rank, we must use the "true" projection matrix (see, e.g., [17]).
3) The CRB becomes unbounded if $C_\delta C_\beta = C_{\delta,\beta}^2$, corresponding to the submatrix becoming singular. When all the subcarriers are active, we have $\mathbf{P}_{\Phi_\mathrm{a}}(\beta) = \mathbf{I}$, and identifiability is lost; in this case, we have $2N+2$ real parameters to estimate from $2N$ real observations.
4) The sensitivity of the signal part $\mathbf{m}_y = \mathbf{D}(\delta)\mathbf{F}_\beta^{\mathcal{H}} \mathbf{T}_\mathrm{a} \boldsymbol{\alpha}$ of the received vector $\mathbf{y}$ with respect to δ and β is $\partial \mathbf{m}_y/\partial\delta = \mathbf{D}(\delta)\mathbf{Q}\mathbf{\Phi}_\mathrm{a}(\beta)\boldsymbol{\alpha}$ and $\partial \mathbf{m}_y/\partial\beta = (N/j2\pi)\mathbf{D}(\delta)\mathbf{Q}\mathbf{\Phi}_\mathrm{a}(\beta)\mathbf{Q}_\mathrm{a}\boldsymbol{\alpha}$. If the variations of $\mathbf{m}_y$ with respect to δ and β are well outside the subspace $\langle \mathbf{D}(\delta)\mathbf{\Phi}_\mathrm{a}(\beta)\rangle$, i.e., on the NSCs, then δ and β can be estimated with low variance. Thus, increasing the number of NSCs, i.e., reducing the number of nuisance parameters in $\boldsymbol{\alpha}$, decreases the CCRB of δ and β. Note that the only difference between $\partial \mathbf{m}_y/\partial\delta$ and $\partial \mathbf{m}_y/\partial\beta$ is that for the $\partial \mathbf{m}_y/\partial\beta$ case, $\boldsymbol{\alpha}$ is weighted by $(N/j2\pi)\mathbf{Q}_\mathrm{a} = \mathrm{diag}[-N_\mathrm{a}/2+1, \ldots, N_\mathrm{a}/2]$. Hence, it is the complex symbols on the highest frequencies that contribute to the variations of $\mathbf{m}_y$ with respect to β.

V. Estimation of Frequency-Offset Parameters

In this section, we will present algorithms for estimating the frequency-offset parameters δ and β. We will consider the deterministic ML (DML) approach and the ESPRIT algorithm.

A. Deterministic ML Approach

When the statistical characteristics of the channel are unknown, it is reasonable to consider the channel parameters $\{H_n\}$ as unknown deterministic parameters. The knowledge of nonzero symbols S_n may be useful for Doppler-estimation, since the channel parameters H_n have far fewer degrees of freedom than the number of active carriers (typically $L \ll N$) [3]; but for reasons of simplicity, we only consider zero pilots (the NSCs). We therefore consider $\alpha_n = H_n S_n$ as unknown deterministic parameters. In this approach, the receiver knows the NSC set, but does not require knowledge of the transmitted symbols.

Assume that the Doppler parameters remain fixed over a block of K OFDM symbols. To cope with the drift in the symbol timing due to a nonzero-rate parameter, we also assume that the cyclic prefix and postfix are sufficiently large such that none of the received OFDM symbols (after discarding the prefix and postfix) contains samples from the previous or next OFDM symbol. Since the additive noise in the model of (5) is assumed to be white, circularly symmetric, and Gaussian, the ML estimates of δ_o, β_o, and $\boldsymbol{\alpha}_o$ are obtained by minimizing the following L_2 norm[1]

$$J(\boldsymbol{\alpha}, \beta, \delta) = \sum_{k=0}^{K-1} \|\mathbf{y}_k - \mathbf{D}(\delta)\mathbf{\Phi}_\mathrm{a}(\beta)\boldsymbol{\alpha}_k\|_2^2 \tag{14}$$

where $\mathbf{\Phi}_\mathrm{a}(\beta)$ is defined in (12). Given that $\mathbf{\Phi}_\mathrm{a}$ is full column rank, the ML estimator of $\boldsymbol{\alpha}_k$, corresponding to a candidate δ and β, is

$$\widehat{\boldsymbol{\alpha}}_k = \mathbf{\Phi}_\mathrm{a}^\dagger(\beta)\mathbf{D}^{\mathcal{H}}(\delta)\mathbf{y}_k \tag{15}$$

[1]We use subscripts o to denote the true parameters; hats will denote estimates. The vector $\boldsymbol{\alpha}$ consists of all the KN_a faded subcarrier symbols. In this multisymbol ML version, there is an additional initial phase shift that depends upon β and δ; this has been absorbed into the faded symbol $\boldsymbol{\alpha}_k$. The estimator is no longer true ML for $K \geq 2$.

where $\mathbf{\Phi}_{\rm a}^{\dagger}(\beta) = (\mathbf{\Phi}_{\rm a}^{\mathcal{H}}(\beta)\mathbf{\Phi}_{\rm a}(\beta))^{-1}\mathbf{\Phi}_{\rm a}^{\mathcal{H}}(\beta)$. Using (15) in (14), the reduced cost function becomes

$$J(\beta,\delta) = -\sum_{k=0}^{K-1} \mathbf{y}_k^{\mathcal{H}}\mathbf{D}(\delta)\mathbf{P}_{\mathbf{\Phi}_{\rm a}(\beta)}\mathbf{D}^{H}(\delta)\mathbf{y}_k$$

where $\mathbf{P}_{\Phi_{\rm a}(\beta)} = \mathbf{\Phi}_{\rm a}(\beta)\mathbf{\Phi}_{\rm a}^{\dagger}(\beta)$ is the projection matrix onto the subspace $\langle\mathbf{\Phi}_{\rm a}(\beta)\rangle$. Since projection matrices are idempotent, the ML estimators of δ_o and β_o are given by

$$\{\hat{\delta}_o,\hat{\beta}_o\} = \arg\max_{\delta,\beta} \mathrm{Tr}\left\{\mathbf{P}_{\Phi_{\rm a}(\beta)}\mathbf{D}^{\mathcal{H}}(\delta)\left[\sum_{k=0}^{K-1}\mathbf{y}_k\mathbf{y}_k^{\mathcal{H}}\right]\mathbf{D}(\delta)\right\}. \tag{16}$$

The DML estimate thus consists of applying a shift corresponding to the candidate frequency offset δ and then projecting the phase-rotated data onto a subspace corresponding to the candidate β. The DML estimates are the ones that maximize the projected energy. In the last equation, the term within the square brackets is an estimate of the time-domain correlation of the received data. When $\beta = 0$ is known, the procedure simplifies to the periodogram-based estimator in [2].

The preceding solution cannot be expressed in closed form, and hence, requires a two-dimensional (2-D) grid search. Let us define $\mathbf{p} = [\delta,\beta]^{\rm T}$ and

$$\widetilde{J}(\mathbf{p}) = \sum_{k=0}^{K-1}\mathbf{y}_k^{\mathcal{H}}\mathbf{D}(\delta)\mathbf{P}^{\perp}_{\mathbf{\Phi}_{\rm a}(\beta)}\mathbf{D}^{\mathcal{H}}(\delta)\mathbf{y}_k \tag{17}$$

where $\mathbf{P}^{\perp}_{\mathbf{\Phi}_{\rm a}(\beta)} = \mathbf{I} - \mathbf{P}_{\Phi_{\rm a}}(\beta)$ is the projection matrix onto the subspace $\langle\mathbf{\Phi}_{\rm a}(\beta)\rangle^{\perp}$, i.e., the subspace orthogonal to $\langle\mathbf{\Phi}_{\rm a}(\beta)\rangle$. Then, a gradient search algorithm is given by

$$\widehat{\mathbf{p}}_{k+1} = \widehat{\mathbf{p}}_k - \mu_k\Re\left\{\frac{\partial\widetilde{J}}{\partial\mathbf{p}}\Big|_{\mathbf{p}=\mathbf{p}_k}\right\} \tag{18}$$

where $\partial\widetilde{J}/\partial\mathbf{p} = [\partial\widetilde{J}/\partial\delta, \partial\widetilde{J}/\partial\beta]^{\rm T}$. Using results in [24], we have

$$\frac{\partial J}{\partial\delta} = \sum_{k=0}^{K-1}\mathbf{y}_k^{\mathcal{H}}\mathbf{D}(\delta)\left(\mathbf{Q}\mathbf{P}^{\perp}_{\mathbf{\Phi}_{\rm a}(\beta)} + \mathbf{P}^{\perp}_{\mathbf{\Phi}_{\rm a}(\beta)}\mathbf{Q}^{\mathcal{H}}\right)\mathbf{D}^{\mathcal{H}}(\delta)\mathbf{y}_k$$

$$\frac{\partial J}{\partial\beta} = \sum_{k=0}^{K-1}\mathbf{y}_k^{\mathcal{H}}\mathbf{D}(\delta)\left[\frac{\partial}{\partial\beta}\mathbf{P}^{\perp}_{\mathbf{\Phi}_{\rm a}(\beta)}\right]\mathbf{D}^{\mathcal{H}}(\delta)\mathbf{y}_k$$

$$= \frac{N}{j2\pi}\sum_{k=0}^{K-1}\mathbf{y}_k^{\mathcal{H}}\mathbf{D}(\delta) \times\left[\left(\mathbf{P}^{\perp}_{\mathbf{\Phi}_{\rm a}(\beta)}\mathbf{Q}\mathbf{\Phi}_{\rm a}(\beta)\mathbf{Q}_{\rm a}\mathbf{\Phi}_{\rm a}^{\dagger}(\beta)\right)^{\mathcal{H}} - \mathbf{P}^{\perp}_{\mathbf{\Phi}_{\rm a}(\beta)}\mathbf{Q}\mathbf{\Phi}_{\rm a}(\beta)\mathbf{Q}_{\rm a}\mathbf{\Phi}_{\rm a}^{\dagger}(\beta)\right]\mathbf{D}^{\mathcal{H}}(\delta)\mathbf{y}_k$$

where we have used (34) in Appendix.

It is very likely that the cost function J contains many local extrema, so that a gradient search may fail with arbitrary initial conditions. To see this, consider the large K case. Then

$$\frac{1}{K}\sum_{k=0}^{K-1}\mathbf{y}_k\mathbf{y}_k^{\mathcal{H}} \approx \mathrm{E}\left\{\mathbf{y}_k\mathbf{y}_k^{\mathcal{H}}\right\} = \mathbf{D}(\delta_o)\mathbf{\Phi}_{\rm a}(\beta_o)\mathbf{\Phi}_{\rm a}^{\mathcal{H}}(\beta_o)\mathbf{D}^{\mathcal{H}}(\delta_o)+\sigma_w^2\mathbf{I} \tag{19}$$

and the cost function in (16) will converge to

$$\lim_{K\to\infty}\frac{J(\delta,\beta)}{K} \propto \mathrm{Tr}\left\{\mathbf{P}_{\Phi_{\rm a}(\beta)}\mathbf{D}(\delta_o-\delta)\mathbf{\Phi}_{\rm a}(\beta_o)\mathbf{\Phi}_{\rm a}^{\mathcal{H}}(\beta_o)\mathbf{D}^{\mathcal{H}}(\delta_o-\delta)\right\}. \tag{20}$$

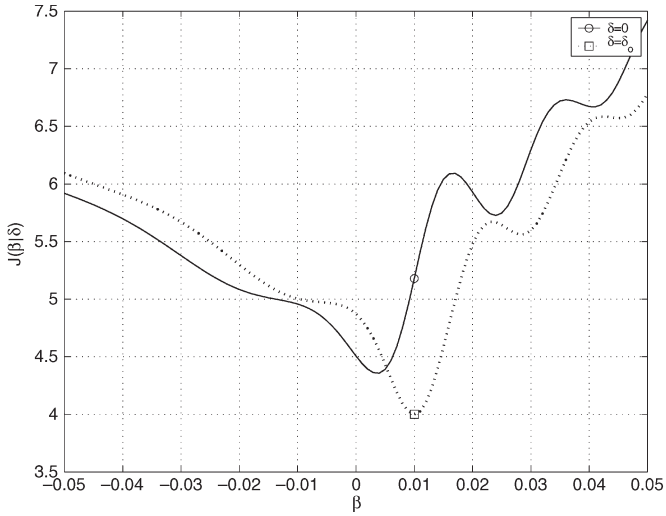

Fig. 5. $J(\beta|\delta)$ as a function of β conditioned on some value of δ. Solid line corresponds to $\delta = 0$, and the dotted one to $\delta = \delta_o$. The true values were $\delta = 0.3, \beta_o = 0.01$.

Fig. 5 shows the cost function J as a function of β conditioned on its true value $\delta = \delta_o = 0.3$ (solid line), and conditioned on $\delta = 0$ (dashed line). Here $\beta_o = 0.01$ and $N = 64$. Clearly, the cost function is highly multimodal. If J is conditioned on a wrong value of δ, the global minimum of $J(\beta|\delta)$ will not be located at β_o. Thus, the MLE will need good initialization. Fig. 6 similarly depicts $J(\delta|\beta)$ corresponding to $\beta = 0$ and $\beta = \beta_o$.

B. Identifiability

The problem with nonidentifiability due to the placement of subcarriers and channel zeros for the CFO-only cases is well treated in [2]. Assume that $K = 1$, then as in the CFO-only case, an obvious necessary condition for identifiability of δ and β is that

$$\boldsymbol{\alpha}^{\mathcal{H}}\boldsymbol{\alpha} \neq 0 \quad\Leftrightarrow\quad \boldsymbol{\alpha} \neq \mathbf{0} \tag{21}$$

which assumes that the signal energy is not zero. If the channel can be modeled as a finite impulse-response (FIR) channel with $L_h + 1$ taps, at most L_h of the H_n's in (3) would be zero, corresponding to the case where all channel zeros are fortuitously at the subcarriers frequencies. The condition in (21) can be satisfied, independent of the channel, if at least $L_h + 1$ subcarriers are activated, i.e., $N_{\rm a} > L_h$.

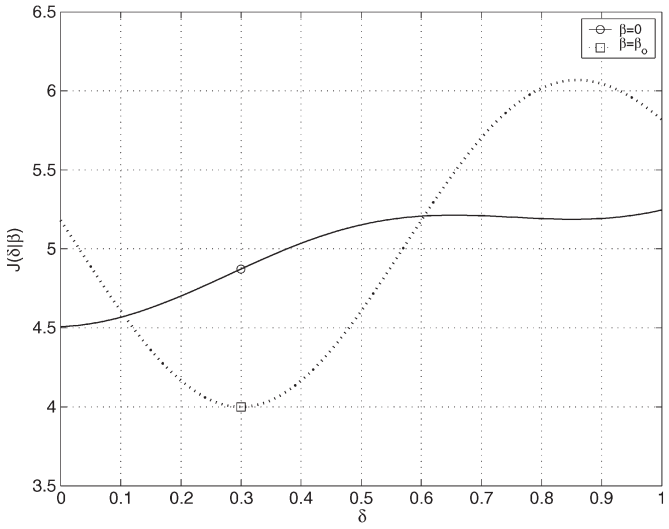

Fig. 6. $J(\delta|\beta)$ as a function of δ conditioned on some value of β. Solid line corresponds to $\beta = 0$, and the dotted one to $\beta = \beta_o$. The true values were $\delta = 0.3$, $\beta_o = 0.01$.

In the noise-free case, we have from (5) and (12), $\mathbf{y} = \mathbf{D}(\delta)\mathbf{\Phi}_{\rm a}(\beta)\boldsymbol{\alpha}$, so that the objective function in (17), with $K = 1$, can be expressed as

$$J(\delta,\beta) = \boldsymbol{\alpha}^{\mathcal{H}}\mathbf{\Phi}^{\mathcal{H}}(\beta_o)\mathbf{D}^{\mathcal{H}}(\delta_o) \times \left[\mathbf{I} - \mathbf{D}(\delta)\mathbf{P}_{\mathbf{\Phi}_{\rm a}(\beta)}\mathbf{D}^{\mathcal{H}}(\delta)\right]\mathbf{D}(\delta_o)\mathbf{\Phi}_{\rm a}(\beta_o)\boldsymbol{\alpha} \quad (22)$$

and the identifiability of the Doppler parameters is lost if there exists an $\boldsymbol{\alpha}$ such that $J(\delta,\beta) = J(\delta_o,\beta_o)$. The frequency response of the channel is $H(f) = \sum_{\ell=0}^{L_h} h[\ell]{\rm e}^{-j2\pi\ell f/N}$, hence, the frequency-response vector $\widetilde{\mathbf{h}} = [H_{-N/2+1} \ \cdots \ H_{N/2}]^{\rm T} = \sqrt{N}\mathbf{F}_\beta^{\rm T}\mathbf{T}_{zp}\mathbf{h} \triangleq \mathbf{V}_\beta\mathbf{h}$, where $\mathbf{T}_{zp} = [\mathbf{I}_{L_h+1}, \mathbf{0}_{L_h+1,N-L_h-1}]^{\rm T}$ pads zeros to the vector $\mathbf{h}$. Note that the frequency-response vector $\widetilde{\mathbf{h}}$ depends on the rate parameter β. Now, we can rewrite $\boldsymbol{\alpha}$ as

$$\boldsymbol{\alpha} = \sqrt{N}\mathbf{D}(\mathbf{s})\mathbf{T}_{\rm a}^{\rm T}\mathbf{F}_\beta\mathbf{T}_{zp}\mathbf{h} \triangleq \mathbf{D}(\mathbf{s})\mathbf{T}_{\rm a}^{\rm T}\mathbf{V}_\beta\mathbf{h} \quad (23)$$

where $\mathbf{D}(\mathbf{s}) = {\rm diag}(\mathbf{s})$, and $\mathbf{s}$ is the symbol vector. Substituting (23) into (22), we see that identifiability is lost if for a given symbol vector $\mathbf{s}$, there exists a channel tap-vector $\mathbf{h}$ such that

$$\left[\mathbf{I} - \mathbf{D}(\delta)\mathbf{P}_{\mathbf{\Phi}_{\rm a}(\beta)}\mathbf{D}^{\mathcal{H}}(\delta)\right]\mathbf{D}(\delta_o)\mathbf{\Phi}_{\rm a}(\beta_o)\mathbf{T}_{\rm a}^{\rm T}\mathbf{V}_\beta\mathbf{h} \triangleq \boldsymbol{\mathcal{G}}\mathbf{h} = \mathbf{0}$$

for $\delta \neq \delta_o$ and $\beta \neq \beta_o$. The diagonal matrix $\mathbf{D}(\mathbf{s})$ has been dropped since the columns of $\mathbf{D}(\delta_o)\mathbf{\Phi}_{\rm a}(\beta_0)\mathbf{D}(\mathbf{s})$ and $\mathbf{D}(\delta_o)\mathbf{\Phi}_{\rm a}(\beta_0)$ span the same subspace. Let

$$d = \dim\left(\mathrm{null}\left\{\boldsymbol{\mathcal{G}}\right\}\right) \quad (24)$$

hence, identifiability is lost if $d > 0$. Following (24), the active-carrier set must be chosen so that $\boldsymbol{\mathcal{G}}$ has full column rank over the range of operational β and δ. Moreover, if $d > 0$, then the intersection between the $L_h + 1$-dimensional subspace $\langle\mathbf{D}(\delta_o)\mathbf{\Phi}_{\rm a}(\beta_o)\mathbf{T}_{\rm a}^{\rm T}\mathbf{V}_\beta\rangle$ and the $N_{\rm a}$-dimensional subspace $\mathrm{null}\{\mathbf{I} - \mathbf{P}_{\mathbf{D}(\delta)\Phi_{\rm a}(\beta)}\} = \langle\mathbf{D}(\delta)\Phi_{\rm a}(\beta)\rangle$ is not empty. This would obviously be the case when $N_{\rm a} + (L_h + 1)$ is larger than N, hence the number of active subcarriers must satisfy $L_h + 1 \leq N_{\rm a} \leq N - (L_h + 1)$. If $\beta = \beta_0$, and if $\delta - \delta_o$ is of the form $m(1+\beta)$, where m is an integer, then the corresponding results derived in [2] also hold here.

C. ESPRIT Approach

The standard ESPRIT algorithm exploits the shift-invariant structure available in some signal subspace and estimates the parameters of interest through subspace decomposition and generalized eigenvalue calculation [5], [15]. The ESPRIT algorithm has been used in [23] to find a closed-form expression for CFO in the $\beta = 0$ case. ESPRIT can be used to provide the initial estimates for the ML estimator. If we define

$$\phi_n = \frac{1}{N}\left[\delta + (1+\beta)n\right] \quad (25)$$

then we can rewrite the received vector in (5) as

$$\mathbf{y} = \mathbf{D}(\delta)\mathbf{\Phi}_a(\beta)\boldsymbol{\alpha} + \mathbf{v} = \mathbf{A}(\boldsymbol{\phi})\boldsymbol{\alpha} + \mathbf{w} \quad (26)$$

where

$$\boldsymbol{\phi} = \left[\phi_{n_1}, \cdots, \phi_{n_{N_{\rm a}}}\right]^{\rm T},$$
$$\mathbf{A}(\boldsymbol{\phi}) = \mathbf{D}(\delta)\mathbf{\Phi}_{\rm a}(\beta) = \left[\mathbf{a}(\phi_{n_1}), \cdots, \mathbf{a}(\phi_{n_{N_{\rm a}}})\right],$$
$$\mathbf{a}(\phi_k) = \frac{1}{\sqrt{N}}\left[1, {\rm e}^{j2\pi\phi_k}, \cdots, {\rm e}^{j2\pi(N-1)\phi_k}\right]^{\rm T}.$$

This is now in a standard array-processing framework corresponding to a uniformly spaced array of N sensors and $N_{\rm a}$ sources. Identifiability demands at least one NSC ($N_{\rm a} < N$). If matrix $\mathbf{A}(\boldsymbol{\phi})$ has full column rank (see Proposition 1), and if the faded-symbol vector $\boldsymbol{\alpha}$ has uncorrelated elements, then we can use standard array-processing techniques.

Let $\mathbf{R}_{yy}$ denote the correlation matrix of $\mathbf{y}$, and let $\mathbf{U}$ denote the set of eigenvectors corresponding to the largest $N_{\rm a}$ eigenvalues. Let $\mathbf{U}_1 \triangleq [\mathbf{I}_{N-1}, \mathbf{0}]\mathbf{U}$, and $\mathbf{U}_2 \triangleq [\mathbf{0}, \mathbf{I}_{N-1}]\mathbf{U}$. Then, following standard ESPRIT, the eigenvalues of the matrix $(\mathbf{U}_1^{\mathcal{H}}\mathbf{U}_1)^{-1}\mathbf{U}_1^{\mathcal{H}}\mathbf{U}_2$ are $\exp(j\phi_n)$, $n \in \mathcal{N}_{\rm a}$. The angles ϕ_n can be obtained from the eigenvalues of $(\mathbf{U}_1^{\mathcal{H}}\mathbf{U}_1)^{-1}\mathbf{U}_1^{\mathcal{H}}\mathbf{U}_2$, provided that $-N/2 < \delta + n(1+\beta) < N/2$, $\forall n \in \mathcal{N}_{\rm a}$. Having estimated the ϕ_n's, β and δ can be obtained as the least-squares solution of (25). In practice, $\mathbf{R}_{yy}$ would be estimated from multiple OFDM symbols.

VI. Numerical Simulations

We will now simulate the proposed MLE and ESPRIT algorithms for the Doppler parameters β and δ. Here, SNR is defined as

$${\rm SNR} = 10\log_{10}\left[\frac{\left(\frac{1}{N_{\rm a}}\right)\sum_{n\in\mathcal{N}_{\rm a}}{\rm E}\left\{|H(n)|^2\,|S(n)|^2\right\}}{\sigma_w^2}\right] \quad (27)$$

where σ_w^2 is the variance of the additive noise.

In all of our simulations, the multipath channel is assumed to be quasi-stationary, i.e., all variations of the channel frequency

response H_n are negligible during transmission of a single OFDM data block.

Recall that the CCRBs in (13) are derived under the assumption that the nuisance parameter $\boldsymbol{\alpha}_n$ is deterministic, but unknown. However, in practice $\boldsymbol{\alpha}_n$ is random since channel and transmitted symbols vary from one OFDM symbol to the next. In order to have a reliable evaluation of the CRB, it is necessary to "average out" the nuisance-parameter vector. A method for doing this is via the extended Miller–Chang bound (EMCB). It follows from the analysis in [4] that

$$\mathrm{EMCB}(\delta,\beta) = \mathrm{E}_{\mathbf{w}_n}\left\{\mathrm{CCRB}(\delta,\beta)\right\}. \tag{28}$$

Since the distribution of $\boldsymbol{\alpha}_n$ cannot be written in closed form, we must rely on Monte Carlo simulation to evaluate $\mathrm{EMCB}(\delta,\beta)$. Both the mean-square error (mse) and the EMCB are estimated empirically from 5000 Monte Carlo runs.

A. ML Estimation

To evaluate the ML estimator, we consider an underwater communication system. In our simulations, we use parameters that are in the same range as the parameters used to describe the channel in [7]. Our main focus will be on estimating and analyzing the performance degradation due to the parameter β, since the performance analysis of the δ-only scenario is well known [11].

Assume that the maximum delay spread is $\tau_{\max} = 29$ ms (corresponds to a path difference of 45 m in the underwater case), and that the Doppler factor β is less than 0.01. This yields a maximum Doppler shift of 100 Hz at the center frequency $f_c = 10$ kHz. The OFDM symbol duration is $T_s = 128$ ms, and the transmission bandwidth is $B = 1/T_c = 2$ kHz. Thus, the number of subcarriers is $N = T_s/T_c = 256$, with subcarrier spacing $\Delta f = B/N \approx 7.8$ Hz, and channel order $L_h = \tau_{\max}/T_c = 60$. We extend the OFDM frame with an overhead in the cyclic prefix, and a postfix of two samples each (see Fig. 1). Hence, the OFDM frame consists of 320 samples in total.

To evaluate the performance of the estimator, we consider two NSC index sets. The first set consists of 48 NSCs placed at the frequency edges of the spectrum, i.e., 24 NSCs on each side. The second set consists of 32 edge NSCs and 16 equispaced NSCs, with NSC index set

$$\mathcal{N}_z = \{-127,\ldots,-112,-99,-86,-72,-59,-46,-33,$$
$$-19,-6,7,20,34,47,60,73,87,100,113,\ldots,128\}. \tag{29}$$

For both sets, the number of active subcarriers is $N_a = 208$.

Fig. 7 shows the EMCB and mse of the estimated (ML) parameters $\widehat{\delta}$ (symbol o) and $\widehat{\beta}$ (symbol $*$) versus SNR using only edge NSCs (solid lines), and the NSC index set in (29) (dashed lines). The dotted lines depict the corresponding EMCB. The data symbols are drawn from a 16-QAM constellation, and the channel coefficients are generated using an uncorrelated Rayleigh scattering model with exponential power-delay profile, i.e., $\mathrm{E}\{h_k^* h_\ell\} = \exp(-\mu k)\delta_{k,\ell}$, with $\mu = 1/5$, $k = 0,\ldots,L_h$, and channel length $L_h = 60$. The Doppler parameters δ and β were generated randomly from $\mathcal{U}[-4,4]$ and $\mathcal{U}[-0.01,0.01]$, respectively. Both channel coefficients and Doppler parameters are generated independently for each Monte Carlo run, and only one OFDM frame ($K = 1$), is used to estimate the Doppler parameters. From Fig. 7, we see that the performance depends strongly on the NSC set. The NSC index set in (29) has much better performance than does the edge NSC set. For the NSC index set in (29), the mse of the Doppler parameters is equal to the EMCB for high SNRs, whereas for low SNRs, the mse deviates slightly from the EMCB. Note also that the estimator applies the constraint that $\delta \in [-4,4]$ and $\beta \in [-0.01,0.01]$, and hence, the mse is less than EMCB for low SNRs when the NSCs are only at the band edges. Clearly, the constrained EMCB will be below the empirical performance. It is difficult to evaluate the EMCB with constraints of this nature, hence, we have provided the more pessimistic unconstrained EMCB.

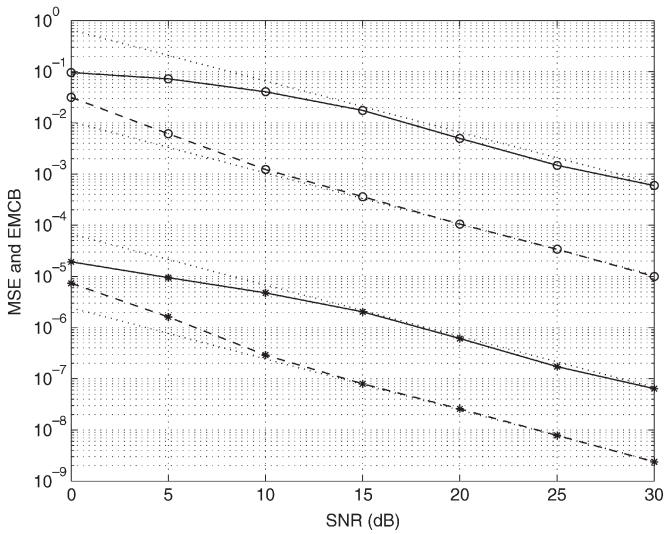

Fig. 7. EMCB and mse of the estimated (ML) Doppler parameters $\widehat{\delta}$ (symbol o) and $\widehat{\beta}$ (symbol $*$) versus SNR using only band-edge NSCs (solid lines), and the NSC index set in (29) (dashed lines). The dotted lines depict the corresponding EMCB.

Fig. 8 shows the mse of the estimated (ML) parameters $\widehat{\delta}$ (symbol o) and $\widehat{\beta}$ (symbol $*$) normalized with respect to $|\beta|$ and $|\delta|$ versus SNR using only edge NSCs (solid lines), and the NSC index set in (29) (dashed lines). The experimental setup is equal to the one used to generate Fig. 7. From Fig. 8, we see that the results are similar to those shown in Fig. 7, i.e., the normalized mse decreases with SNR as expected.

When the receiver ignores the presence of the rate parameter β, and assumes it is equal to zero, then the CFO δ is estimated as

$$\widehat{\delta} = \arg\max_{\delta} \sum_{k=0}^{K-1} \mathbf{y}_k^{\mathcal{H}} \mathbf{D}(\delta)\mathbf{F}_0^{\mathcal{H}}\mathbf{T}_a\mathbf{T}_a^{\mathrm{T}}\mathbf{F}_0\mathbf{D}^{\mathcal{H}}(\delta)\mathbf{y}_k \tag{30}$$

where $\mathbf{y}_k = \mathbf{D}(\delta_o)\boldsymbol{\Phi}_a(\beta_o)\boldsymbol{\alpha}_k + \mathbf{w}$.

Fig. 9 shows mse of the estimated (ML) CFO $\widehat{\delta}$ using (30) versus SNR, evaluated for a true β_o equal to 0 (solid line), 1/1000 (symbol o), 1/500 (symbol $*$), and 1/150 (symbol $\times$). The data symbols are drawn from a 16-QAM constellation,

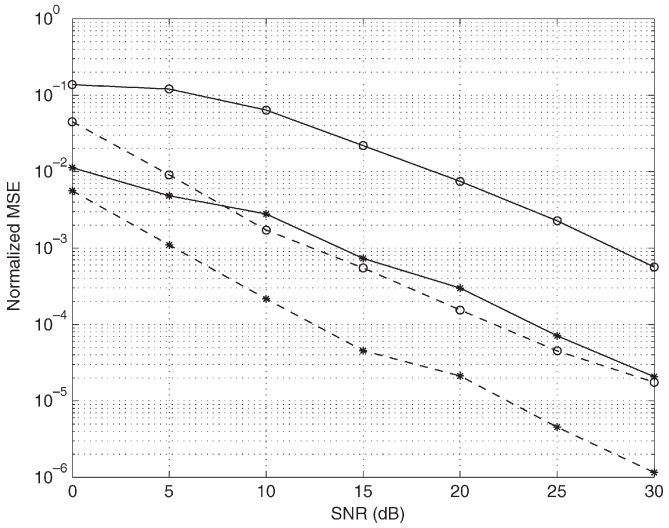

Fig. 8. Normalized mse of the estimated (ML) Doppler parameters $\widehat{\delta}$ (symbol o) and $\widehat{\beta}$ (symbol $*$) versus SNR using only band-edge NSCs (solid lines), and the NSC index set in (29) (dashed lines).

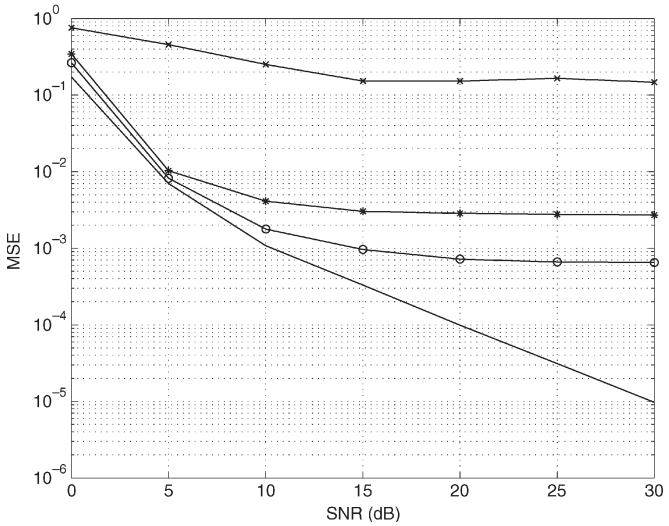

Fig. 9. mse of the estimated (ML) CFO parameters $\widehat{\delta}$ versus SNR evaluated for a true β_o equal to 0 (solid line), 1/1000 (symbol o), 1/500 (symbol $*$), and 1/150 (symbol $\times$).

and the channel coefficients are generated as in the previous example. The CFO parameter δ was generated randomly from $\mathcal{U}[-4,4]$, and the NSCs were selected from the index set in (29). From the figure, we see that performance degrades when the receiver ignores the rate parameter β. Note also that the performance degradation is more significant for high SNR. However, since δ is chosen from the interval $[-4,4]$, the estimator in (30) still provides a coarse estimate of the CFO.

B. ESPRIT Algorithm

We now consider an RF communication system, where the rate parameter β is due to a sampling-rate offset. The number of subcarriers is $N=64$, and the channel order is $L_h=4$. We extend the cyclic prefix and postfix in the OFDM frame with

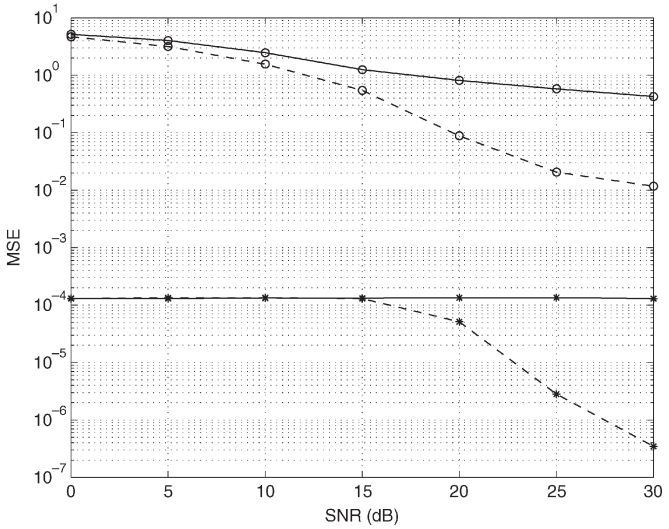

Fig. 10. mse of the estimated (ESPRIT) Doppler parameters $\widehat{\delta}$ (symbol o) and $\widehat{\beta}$ (symbol $*$) versus SNR. Solid lines depict the mse for edge NSCs only, and dashed lines depict the mse for the NSC set given in (31).

nine samples each to accommodate for a drift in the symbol timing. Hence, the OFDM frame consists of 86 samples in total.

Since the correlation matrix of $\mathbf{y}$ is unknown, we use the sample correlation matrix $\widehat{\mathbf{R}}_y$. To estimate $\widehat{\mathbf{R}}_y$, we use the method suggested by Tureli *et al.* in [23]. Given an OFDM vector $\mathbf{y}_k$, we form $N-M$ blocks of $M+1 \leq N_{\rm a}+1$ consecutive samples in both the forward and backward directions. With K OFDM symbols, we obtain $2K(N-M)$ blocks, which is used to form an estimate of the $(M+1)\times(M+1)$ correlation matrix $\widehat{\mathbf{R}}_{M+1}$. It can be shown [23] that by exploiting the shift-invariant data structure of the OFDM symbols, the eigenvectors that span the signal subspace can be obtained from $\mathbf{R}_{M+1}$. However, for $\widehat{\mathbf{R}}_{M+1}$ to have rank $N_{\rm a}$ (in the noise-free case), we require that the selection of K should be done considering the estimation accuracy, and frequency and timing drifts. If K is too small, the sample correlation matrix will not span the signal subspace, and if it is too large, the estimator will be sensitive to model errors due to the drift in the symbol timing, and the frequency offsets. We choose $K=10$, $N_{\rm a}=52$, and $M=60$.

To evaluate the performance of the estimator, we consider two NSC index sets. The first set consists of 12 NSCs placed at the frequency edges of the spectrum, i.e., six NSCs on each side. The second set consists of eight edge NSCs and four equispaced NSCs with index set

$$\mathcal{N}_z = \{-31,-30,-29,-28,-17,-5,6,18,29,30,31,32\}. \tag{31}$$

Fig. 10 shows the mse of the estimated (ESPRIT) parameters $\widehat{\delta}$ (symbol o), and $\widehat{\beta}$ (symbol $*$) versus SNR using only edge NSCs (solid lines), and the NSC index set given in (31) (dashed lines). Parameters δ and β were generated randomly from $\mathcal{U}[-4,4]$ and $\mathcal{U}[-0.01,0.01]$, respectively. The data symbols are drawn from a 16-QAM constellation, and the channel coefficients were generated as in the previous example, but with $L_h=4$. A random channel was independently generated for each of the $K=10$ OFDM symbols.

We observe that the performance of the ESPRIT estimator depends strongly on the NSC set used; the NSC index set in (31) yields better performance than the edge-only NSC set. However, since the estimator applies the constraint that $\delta \in [-4, 4]$ and $\beta \in [-0.01, 0.01]$, we see that for the edge-only NSCs, the mse of β is constant and equal to 1.31×10^{-4}, whereas for the NSC index set in (31), the ESPRIT estimator performs better for SNR larger than 15 dB. Note that for the edge-only NSCs, the estimator $\widehat{\beta} = 0$, which gives an mse equal to 3.33×10^{-5}, performs better than the ESPRIT algorithm.

VII. Conclusion

In this paper, we analyzed the effect of synchronization errors in wideband OFDM. We showed that both a shift and a rate parameter are required for an adequate description. We derived a model for the received OFDM signal, and showed that it also accommodates a sampling frequency offset. The CRB and ML estimators of the synchronization parameters were derived, and the vector formulation was recast as an ESPRIT estimation problem. Simulations showed that compensation for the rate parameter is mandatory, in order to achieve satisfactory BER results. The ML estimators of δ and β achieved very good performances in terms of their mses. In fact, in the high SNR region, the mse is nearly identical with the EMCB, whereas for lower SNRs, the performance degradation compared to the EMCB is only marginal. The ESPRIT algorithm gives a closed-form estimator for the Doppler parameters, but suffers due to its suboptimality.

Appendix

Let $\overline{\boldsymbol{\alpha}}_k$ and $\widetilde{\boldsymbol{\alpha}}_k$ denote the real and imaginary part of $\boldsymbol{\alpha}_k$, respectively. The parameter vector describing the signal is then $\boldsymbol{\theta} = [\overline{\boldsymbol{\alpha}}_0^{\mathrm{T}}, \widetilde{\boldsymbol{\alpha}}_0^{\mathrm{T}}, \cdots, \overline{\boldsymbol{\alpha}}_{K-1}^{\mathrm{T}}, \widetilde{\boldsymbol{\alpha}}_{K-1}^{\mathrm{T}}, \delta, \beta]^{\mathrm{T}}$. Since we assume that the $\boldsymbol{\alpha}_k$'s are deterministic quantities, the mean vector and covariance matrix of $\mathbf{y} = [\mathbf{y}_0, \mathbf{y}_1, \cdots, \mathbf{y}_{K-1}]^{\mathrm{T}}$ are

$$\mathbf{m} = [\mathbf{D}(\delta)\boldsymbol{\Phi}_{\mathrm{a}}(\beta)\boldsymbol{\alpha}_0, \cdots, \mathbf{D}(\delta)\boldsymbol{\Phi}_{\mathrm{a}}(\beta)\boldsymbol{\alpha}_{K-1}]^{\mathrm{T}} \quad (32)$$

$$\mathbf{R}_y = \sigma_w^2 \mathbf{I}. \quad (33)$$

Using the fact that

$$\frac{\partial \boldsymbol{\Phi}_{\mathrm{a}}(\beta)}{\partial \delta} = \mathbf{Q}\mathbf{D}(\delta) \quad \text{and} \quad \frac{\partial \boldsymbol{\Phi}_{\mathrm{a}}(\beta)}{\partial \beta} = \frac{N}{j2\pi}\mathbf{Q}\boldsymbol{\Phi}_{\mathrm{a}}(\beta)\mathbf{Q}_{\mathrm{a}} \quad (34)$$

the partial derivatives of the mean vector $\mathbf{m}_x$ with respect to the unknown parameters are

$$\frac{\partial \mathbf{m}}{\partial \delta} = [\mathbf{Q}\mathbf{D}(\delta)\boldsymbol{\Phi}_{\mathrm{a}}(\beta)\boldsymbol{\alpha}_0, \ldots, \mathbf{Q}\mathbf{D}(\delta)\boldsymbol{\Phi}_{\mathrm{a}}(\beta)\boldsymbol{\alpha}_{K-1}]^{\mathrm{T}} \quad (35)$$

$$\frac{\partial \mathbf{m}}{\partial \beta} = \frac{N}{j2\pi}[\mathbf{Q}\mathbf{D}(\delta)\boldsymbol{\Phi}_{\mathrm{a}}(\beta)\mathbf{Q}_{\mathrm{a}}\boldsymbol{\alpha}_0, \cdots, \mathbf{Q}\mathbf{D}(\delta)\boldsymbol{\Phi}_{\mathrm{a}}(\beta)\mathbf{Q}_{\mathrm{a}}\boldsymbol{\alpha}_{K-1}]^{\mathrm{T}} \quad (36)$$

$$\frac{\partial \mathbf{m}^{\mathcal{H}}}{\partial \overline{\boldsymbol{\alpha}}_\ell} = \delta_{k,\ell}\boldsymbol{\Phi}_{\mathrm{a}}^{\mathcal{H}}(\beta)\mathbf{D}^{\mathcal{H}}(\delta) \quad (37)$$

$$\frac{\partial \mathbf{m}^{\mathcal{H}}}{\partial \widetilde{\boldsymbol{\alpha}}_\ell} = -j\delta_{k,\ell}\,\boldsymbol{\Phi}_{\mathrm{a}}^{\mathcal{H}}(\beta)\mathbf{D}^{\mathcal{H}}(\delta). \quad (38)$$

We use this in a standard FIM expression (e.g., [6])

$$[\mathbf{J}]_{\theta_k,\theta_\ell} = 2\Re\left\{\frac{\partial \mathbf{m}^{\mathcal{H}}}{\partial \theta_k}\mathbf{R}_y^{-1}\frac{\partial \mathbf{m}}{\partial \theta_\ell}\right\} = \frac{2}{\sigma_w^2}\Re\left\{\frac{\partial \mathbf{m}^{\mathcal{H}}}{\partial \theta_k}\frac{\partial \mathbf{m}}{\partial \theta_\ell}\right\}. \quad (39)$$

After some tedious manipulations, we obtain (13). Because of space limitations, we refer the reader to [17] for the detailed proof. ■

References

[1] J. Balakrishnan, R. K. Martin, and C. R. Johnson, Jr., "Blind, adaptive channel shortening by sum-squared auto-correlation minimization (SAM)," *IEEE Trans. Signal Process.*, vol. 51, no. 12, pp. 3086–3093, Dec. 2003.

[2] M. Ghogho, A. Swami, and G. B. Giannakis, "Optimized null-subcarrier selection for CFO estimation in OFDM over frequency-selective fading channels," in *Proc. IEEE Global Telecommunications (GLOBECOM)*, San Antonio, TX, 2001, vol. 1, pp. 202–206.

[3] M. Ghogho and A. Swami, "Semi-blind frequency offset synchronization for OFDM," in *Proc. Int. Conf. Acoustics, Speech, Signal Processing*, Orlando, FL, May 2002, vol. 3, pp. 2333–2336.

[4] F. Gini and R. Reggiannini, "On the use of Cramer–Rao-like bounds in the presence of random nuisance parameters," *IEEE Trans. Commun.*, vol. 48, no. 12, pp. 2120–2126, Dec. 2000.

[5] D. H. Johnson and D. E. Dudgeon, *Array Signal Processing: Concepts and Techniques*. Englewood Cliffs, NJ: Prentice-Hall, 1993.

[6] S. M. Kay, *Fundamentals of Statistical Signal Processing: Estimation Theory*. Englewood Cliffs, NJ: Prentice-Hall, 1993.

[7] B. Kim and I. Lu, "Parameter study of OFDM underwater communications system," in *Proc. IEEE Oceans*, Providence, RI, Sep. 2000, vol. 2, pp. 1251–1255.

[8] X. Ma, C. Tepedelenlioğlu, G. B. Giannakis, and S. Barbarossa, "Non-data-aided carrier offset estimators for OFDM with null subcarriers: Identifiability, algorithms, and performance," *IEEE J. Sel. Areas Commun.*, vol. 19, no. 12, pp. 2504–2515, Dec. 2001.

[9] P. J. W. Melsa, R. C. Younce, and C. E. Rohrs, "Impulse response shortening for discrete multitone transceivers," *IEEE Trans. Commun.*, vol. 44, no. 12, pp. 1662–1672, Dec. 1996.

[10] R. van Nee and R. Prasad, *OFDM for Wireless Multimedia Communications*. Boston, MA: Artech House, 2000.

[11] T. Pollet, M. van Bladel, and M. Moeneclaey, "BER sensitivity of OFDM systems to carrier frequency offset and Wiener phase noise," *IEEE Trans. Commun.*, vol. 43, no. 2–4, pp. 191–193, Feb.–Apr. 1995.

[12] T. Pollet, P. Spruyt, and M. Moeneclaey, "The BER performance of OFDM systems using non-synchronized sampling," in *Proc. Global Telecommunications (GLOBECOM)*, San Fransico, CA, Nov./Dec. 1994, vol. 1, pp. 253–257.

[13] D. Porcino and W. Hirt, "Ultra-wideband radio technology: Potential and challenges ahead," *IEEE Commun. Mag.*, vol. 41, no. 7, pp. 66–74, Jul. 2003.

[14] J. C. Proakis, E. M. Sozer, J. A. Rice, and M. Stojanovic, "Shallow water acoustic networks," *IEEE Commun. Mag.*, vol. 39, no. 11, pp. 114–119, Nov. 2001.

[15] R. Roy and T. Kailath, "ESPRIT—Estimation of signal parameters via rotational invariance techniques," *IEEE Trans. Acoust., Speech, Signal Process.*, vol. 37, no. 7, pp. 984–995, Jul. 1989.

[16] A. B. Salberg and A. Swami, "Doppler and frequency-offset synchronization in wideband OFDM: Estimators & performance analysis," in *Proc. 5th Nordic Signal Processing Symp.*, Hurtigruten Tromsø-Trondheim, Norway, Oct. 2002. ISBN 8299315840.

[17] A. B. Salberg, "Stochastic multipulse-PAM and issues of synchronization in OFDM," Ph.D. dissertation, Dept. of Physics, Univ. Tromsø, Tromsø, Norway, 2003.

[18] H. Sari, G. Karam, and I. Jeanclaude, "Transmission techniques for digital terrestrial TV broadcasting," *IEEE Commun. Mag.*, vol. 33, no. 2, pp. 100–109, Feb. 1995.

[19] B. S. Sharif, J. Neasham, O. R. Hinton, and A. E. Adams, "A computationally efficient Doppler compensation system for underwater acoustic communications," *IEEE J. Ocean. Eng.*, vol. 25, no. 1, pp. 52–61, Jan. 2000.

[20] M. Speth, S. A. Fechtel, G. Fock, and H. Meyr, "Optimum receiver design for wireless broad-band systems using OFDM—Part I," *IEEE Trans. Commun.*, vol. 47, no. 11, pp. 1668–1677, Nov. 1999.

[21] ——, "Optimum receiver design for wireless broad-band systems using OFDM—Part II," *IEEE Trans. Commun.*, vol. 49, no. 4, pp. 571–578, Apr. 2001.
[22] B. Stantchev and G. Fettweis, "Time-variant distortions in OFDM," *IEEE Commun. Lett.*, vol. 4, no. 10, pp. 312–314, Oct. 2000.
[23] U. Tureli, H. Liu, and M. D. Zoltowski, "OFDM blind carrier offset estimation: ESPRIT," *IEEE Trans. Commun.*, vol. 48, no. 9, pp. 1459–1461, Sep. 2000.
[24] M. Viberg, B. Ottersen, and T. Kailath, "Detection and estimation in sensor arrays using weighted subspace fitting," *IEEE Trans. Signal Process.*, vol. 39, no. 11, pp. 2436–2449, Nov. 1991.

Arnt-Børre Salberg (M'03) received the Diploma degree in applied physics and the Dr. Scient. degree in physics from the University of Tromsø, Tromsø, Norway, in 1998 and 2003, respectively.

He was a Research Scholar with the Department of Physics, University of Tromsø, from January 1999 to January 2003. From August 2001 to June 2002, he was a Visiting Researcher with the US Army Research Laboratory, Adelphi, Maryland. Since February 2003, he has had a Postdoctoral Researcher position at the Observation Methodology Group, Institute of Marine Research, Tromsø, Norway. His research interests are in the area of signal and image processing, pattern recognition, computer vision, and digital communications.

Ananthram Swami (S'79–M'79–SM'96) received the B.S. degree from the Indian Institute of Technology, Bombay, India, the M.S. degree from Rice University, Houston, TX, and the Ph.D. degree from the University of Southern California, Los Angeles, all in electrical engineering.

He has held positions with Unocal Corporation, the University of Southern California, CS-3, and Malgudi Systems. He is currently a Senior Research Scientist with the US Army Research Lab, Adelphi, MD, where his work is in the broad area of signal processing for communications. He was a Statistical Consultant to the California Lottery, developed a Matlab-based toolbox for non-Gaussian signal processing, and has held visiting faculty positions at Institut National Polytechnique (INP), Toulouse, France.